Int. J. Heat Mass Transfer. Vol. 35, No. 5, pp. 1229–1245, 1992
Printed in Great Britain

0017–9310/92 $5.00 + 0.00

Modeling of turbulent transport and solidification during continuous ingot casting

W. SHYY,† Y. PANG,‡ G. B. HUNTER,§ D. Y. WEI‡ and M.-H. CHEN†

† Department of Aerospace Engineering, Mechanics and Engineering Science, University of Florida, Gainesville, FL 32611, U.S.A., ‡ GE Aircraft Engines, Engineering Materials Technology Laboratories, Lynn, MA 01910, U.S.A., § GE Aircraft Engines, Engineering Materials Technology Laboratories, Cincinnati, OH 45215-6301, U.S.A.

(*Received* 26 *February* 1991 *and in final form* 1 *May* 1991)

Abstract—Continuous ingot casting is an important processing technology for many materials. Under most practical circumstances, turbulence plays a critical role which, along with transport mechanisms such as buoyancy, surface tension, and phase change, is responsible for the quality of the end products. A modified turbulence model based on the standard k–ε two-equation closure is proposed and applied to predict the phase change and convection–diffusion characteristics during titanium alloy ingot casting in an electron beam melting process. In conjunction with an adaptive grid computational technique, solutions of the coupled mass continuity, momentum, energy, and turbulence transport have been obtained in the context of the enthalpy formulation. Effects of casting speed and gravity on solidification and convection characteristics have been investigated and compared to ones obtained previously with a simple zero-equation turbulence model. The present turbulence model predicts that the mushy zone is generally of substantial thickness as a result of the convection effect, that the solidus line has a high curvature, and that the temperature gradient close to the solidus line is higher than elsewhere. Under all conditions, the turbulence structure largely reflects the combined influence of convection and energy input by the electron beam and the superheated feeding material from the top surface. The numerical results have been compared with an experimentally determined pool profile from a casting ingot.

1. INTRODUCTION

SIGNIFICANT effort has recently been devoted to the development of processing techniques to produce premium quality crystals and metal alloys for high performance aerospace applications [1, 2]. However, commercial realization of new materials and processes never occurs without first accumulating extensive understanding and insight. Since many materials under development are fundamentally new, existing knowledge and design experience derived from the presently available conventional technologies cannot satisfactorily serve the need. Accordingly, intensive activities have been generated in the research and development community to develop advanced modeling tools for enhancing both qualitative and quantitative understanding of process physics. It is hoped that by combining the new insight and accumulated knowledge from conventional approaches, more advanced processing technologies can be developed and new, high performance materials produced [3].

One of the major melt-related defects in as-cast ingots of high performance metal alloys, such as those based on titanium and nickel, is macrosegregation. Macrosegregation defects, such as 'tree-ring' in nickel-base superalloys, are often formed by abrupt changes to the solidification parameters in the final melt processing step, namely ingot casting [2]. Others, such as 'type II hard alpha' and 'beta flecks' in titanium alloys, form under specific solidification conditions [4]. Type II hard alpha is normally attributed to the segregation of alpha stabilizing alloy elements such as Al and has been associated with ingot pipe formation. Beta flecks are regions of lower beta phase transformation temperature that usually exhibit alpha denuded, larger beta grains in the alpha–beta matrix. They contain higher concentrations of beta-stabilizing elements such as Cr and Fe, and lower concentrations of alpha-stabilizing elements such as Al and O. Such beta fleck segregation patterns have been associated with equiaxed microstructures. Macrosegregation can degrade the properties of jet engine rotating components such as disks, spools and shafts resulting in premature component retirement or failure. Therefore, adequate control of process parameters must be established to eliminate unacceptable segregation patterns.

One of the most influential process variables in controlling the cast microstructure and segregation is the movement of the solidification interface and its associated thermal gradient during the phase change process. Furthermore, the normal operating conditions of these processes are such that many transport mechanisms are present in the solidification process, including buoyancy-induced convection, surface tension-induced (Marangoni) convection, turbulence,

combined conduction–radiation heat transfer, and, most critically, their interactions with the movement of the solidification front. Numerous attempts to understand the general characteristics of these mechanisms have been made during the past several decades, both theoretically and experimentally, as reviewed in refs. [5–8].

Fruitful research has progressed for single crystal growth [7, 9] and welding [10], along with more generic studies conducted by both the finite difference/finite volume [11–15] and the finite element [16, 17] methods to investigate the solidification problems involving convection. A literature survey, however, indicates that very little detailed information is available on simultaneously accounting for phase change along with fluid flow and heat transfer in ingot casting. Earlier studies on ingot casting processes such as Vacuum Arc Remelting (VAR), Electroslag Remelting (ESR), and Electron Beam Melting (EBM) have strictly relied on a classical phase change conduction formulation to determine the location of the mushy region and temperature distribution under various external cooling arrangements [4, 18]. The effect of convection was not explicitly accounted for; it was approximated by boosting the values of molecular thermal conductivity by two to three orders of magnitude.

In an earlier effort [19], physical models and numerical techniques have been assembled to perform computational simulation to delineate the effects of heat diffusion, surface tension, and buoyancy on the transport phenomena and solidification during a Ti–6Al–4V alloy ingot casting process. Although the turbulence effect is included, the treatment is extremely simple, using a linear variation between eddy and molecular values of both viscosity and thermal conductivity. The ratio correlates directly with the local mean fluid temperature, varying from 1 at the solidus temperature to 100 at the liquidus temperature. This approach is a result of a compromise made between attempting first to develop appropriate numerical capabilities to predict qualitative features under the modeling conditions, or to develop a detailed model of mushy zone convection. It must be realized that information regarding the turbulence characteristics even in a pure isothermal melt is sparse [20], not to mention in systems containing the interactions among surface tension, buoyancy, and phase change with the existence of a mushy zone.

In the present work, further effort has been made to develop a more comprehensive turbulence model. The model is based on the k–ε two-equation closure [21] along with the concept of low Reynolds number modification [22] to account for the presence of dendrite branches and phase change in the mushy zone. With this new development, detailed investigation can be made to study the structure of turbulent transport during the ingot casting process, and its impact on the phase change characteristics under both normal gravity and microgravity conditions. As is presented herein, this turbulence model can handle the phase change and the mushy zone formation. It also yields a nonuniform temperature distribution between the solid and liquid phases. Consequently, although the mushy zone is thicker due to convection, the temperature gradient near the solidus line remains high. This latter feature seems to be observed in directionally solidified superalloys [23]. Computationally, a curvilinear coordinate system with an adaptive grid method is utilized in order to help optimize the spatial resolution of the various length scales present in the system.

2. PROBLEM FORMULATION AND NUMERICAL PROCEDURE

An EBM casting process has been chosen to illustrate the numerical procedure. A schematic illustration of the overall system is given in Fig. 1(a), where the raw materials are initially melted with an external heat source in a water-cooled melting hearth before the molten metal is cast into ingots. The modeled geometry as well as conditions of the ingot casting are sketched in Fig. 1(b). For the case considered, the material used is Ti–6Al–4V, with an ingot diameter of 0.432 m, and a height of the copper mold of 0.457 m.

The axisymmetric computational domain includes the liquid, solid and mushy regions of the ingot, with a length-to-diameter aspect ratio of 4. The characteristics of the combined convection–conduction–radiation–solidification process are complicated. Some aspects of the process are either not well understood or too complicated to be handled at a rigorous and fundamental level with current technology. However, efforts have been made to minimize the degrees of *ad hoc* treatments so that essential features of the problem under investigation can be captured adequately.

In practice, the molten material is poured continuously into the copper mold at one circumferential position while the ingot is periodically withdrawn in the vertically downward direction. As we discuss in detail below, the fluid flow appears to be intrinsically turbulent under the present operating conditions, hence a quasi-stationary formulation with eddy viscosity and thermal conductivity accounting for turbulence effect is made. Because of the restrictions of axisymmetry, the feeding mass flow is modeled as entering the mold in an annular ring at a constant rate. The ingot withdrawal is modeled as a steady and continuous movement at a constant casting speed, u_{cast}. The value of u_{cast} is calculated based on the dimensions and density of the solidified material and the feeding mass flow rate from the top.

As to the convection mechanisms, the buoyancy effect within the melt and thermocapillary effect on the pool surface have been included in the present model. In estimating the strength of buoyancy-induced convection, one can use the Rayleigh number,

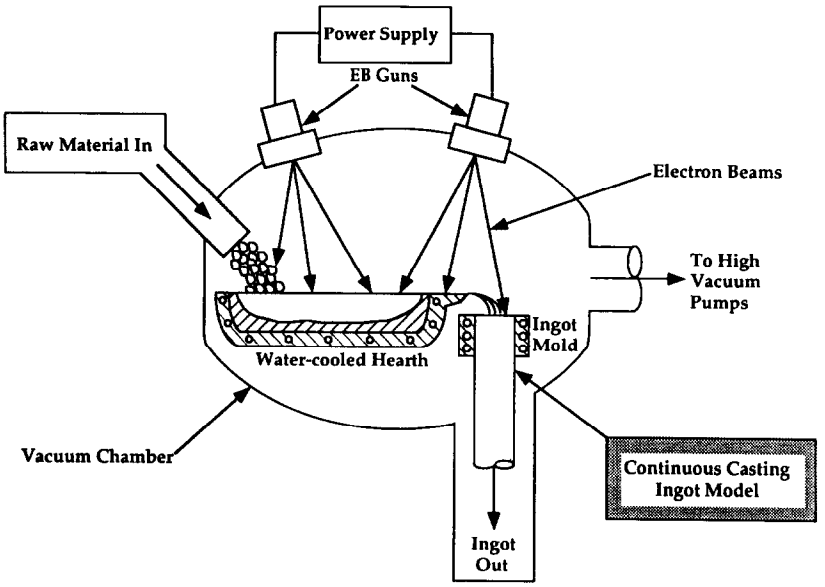

FIG. 1(a). Schematic of cold hearth EBM ingot casting system.

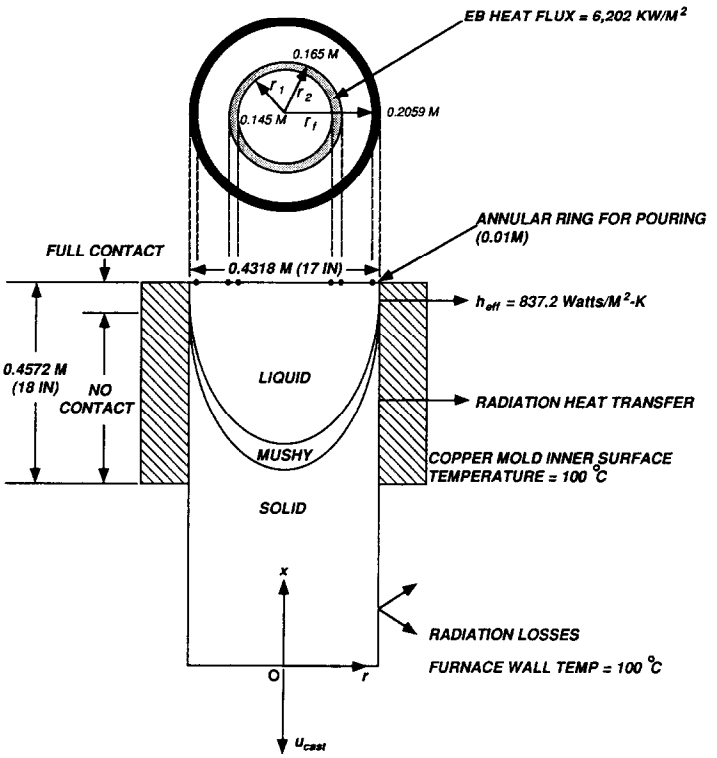

FIG. 1(b). Ingot model schematic and boundary conditions.

Ra, as an indicator. The Rayleigh number is defined as

$$Ra = Gr \cdot Pr$$

where Gr and Pr are, respectively, the Grashof and Prandtl numbers, defined as

$$Gr = \frac{gl^3\Delta\rho}{\nu^2\rho}, \quad Pr = \frac{\nu}{\alpha}$$

where l is a characteristic length scale, ν and α are,

respectively, the kinematic viscosity and thermal diffusivity of the molten alloy, ρ and $\Delta\rho$ are, respectively, the reference density of the molten alloy and its variation, and g is gravitational acceleration. Here, we choose the characteristic length l to be the ingot radius, $R = 0.216$ m, and the representative kinematic viscosity to be the value at the liquidus temperature, T_{liq} (1898 K), which is about 10^{-6} m^2 s^{-1}. Hence, under the normal gravity level observed on earth

$$Gr \sim 10^{11}\frac{\Delta\rho}{\rho}.$$

The Prandtl number at T_{liq} is 0.165, resulting in a Rayleigh number of

$$Ra \sim 10^{10}\frac{\Delta\rho}{\rho}.$$

It is emphasized here that although the casting material temperatures generally increase from bottom to top, their nonuniform distributions along the radial direction can still cause an imbalanced density field to produce buoyancy-induced convection. Our calculations indicated that the density imbalance $\Delta\rho/\rho$ could be around 10%, yielding a Rayleigh number of the order of 10^9. Regarding the thermocapillary aspect, based on the same length scale and the material properties given in Table 1, it is estimated that the Marangoni number is of the order of 10^6. Hence, the flows are well within the turbulent regime.

The Favre-averaged Navier–Stokes equations of mass continuity, momentum, and energy transport, along with a modified k–ε two-equation turbulence closure, are the basis of our computations. We have adopted the enthalpy formulation to represent both liquid and solid phases within a unified set of equations. In terms of the momentum equations, a Darcy's law type of porous medium treatment is utilized to account for the effect of phase change on convection. The equations are written in cylindrical coordinates in order to handle the axisymmetric problems; they are given in the following:

(i) Continuity

$$\frac{\partial}{\partial x}(r\rho(u+u_{cast}))+\frac{\partial}{\partial r}(r\rho v)=0$$

where u_{cast} is the casting speed, which is incorporated as a constant advection speed.

(ii) u-Momentum (along the axial x-direction)

$$\frac{1}{r}\left[\frac{\partial}{\partial x}(r\rho(u+u_{cast})u)+\frac{\partial}{\partial r}(r\rho uv)\right]$$
$$=-\frac{\partial p}{\partial x}+\frac{1}{r}\left[\frac{\partial}{\partial x}\left(r\mu_t\frac{\partial u}{\partial x}\right)+\frac{\partial}{\partial r}\left(r\mu_t\frac{\partial u}{\partial r}\right)\right]+Au+\rho g$$

where p is pressure and μ_t is the eddy viscosity. The coefficient $A = -C(1-\lambda)^2/\lambda^3$, with λ being the fraction of liquid which is equal to 1 in liquid, 0 in solid, and varies linearly with temperature in the mushy zone. The formula adopted here is the same as the Carman–Kozeny form and the value of the Darcy coefficient C needs to be determined according to the material structures.

(iii) v-Momentum (along the radial r-direction)

$$\frac{1}{r}\left[\frac{\partial}{\partial x}(r\rho(u+u_{cast})v)+\frac{\partial}{\partial r}(r\rho v^2)\right]=-\frac{\partial p}{\partial r}$$
$$+\frac{1}{r}\left[\frac{\partial}{\partial x}\left(r\mu_t\frac{\partial v}{\partial x}\right)+\frac{\partial}{\partial r}\left(r\mu_t\frac{\partial v}{\partial r}\right)\right]-\frac{2\mu_t v}{r^2}+Av.$$

(iv) Energy equation (based on sensible enthalpy ϕ and latent heat content ΔH)

$$\frac{1}{r}\left[\frac{\partial}{\partial x}(r\rho(u+u_{cast})\phi)+\frac{\partial}{\partial r}(r\rho v\phi)\right]$$
$$=\frac{1}{r}\left[\frac{\partial}{\partial x}\left(rk_t\frac{\partial T}{\partial x}\right)+\frac{\partial}{\partial r}\left(rk_t\frac{\partial T}{\partial r}\right)\right]$$
$$-\frac{1}{r}\left[\frac{\partial}{\partial x}(r\rho(u+u_{cast})\Delta H)+\frac{\partial}{\partial r}(r\rho v\Delta H)\right]$$

Table 1. Values of important material and process parameters

Surface tension coefficient	$\partial\gamma/\partial T = -2.7\times10^{-4}$ N m^{-1} K^{-1}
Emissivity of solid	$\varepsilon_{sol} = 0.4$
Emissivity of liquid	$\varepsilon_{liq} = 0.2$
Ambient background temperature	$T_{amb} = 373$ K
Mold temperature	$T_{mold} = 373$ K
Effective heat transfer coefficient	$h_{eff} = 837.2$ W m^{-2} K^{-1}
Latent heat	$\Delta H_f = 3.183\times10^5$ J kg^{-1}
Liquidus temperature	$T_{liq} = 1898$ K
Solidus temperature	$T_{sol} = 1868$ K
Darcy coefficient	$C = 10^6$ s^{-1}
Gravitational acceleration	$g_0 = -9.8$ m s^{-2}
Heat flux from electron beam	$q_{beam} = 6.22\times10^6$ W m^{-2}
Temperature of material poured into mold	$T_i = 1998$ K

where T is temperature, k_t is eddy thermal conductivity, $\Delta H = \lambda \Delta H_f$ and ΔH_f is the latent heat of 100% liquid.

(v) Turbulence closure. A major objective in the present work is to develop and apply a low Reynolds number version of k–ε two-equation closure capable of handling the turbulence effect both within the bulk melt and across the mushy zone. Because of the modification of the Navier–Stokes equations made by Darcy's terms, the velocity field in the mushy zone does not yield information to distinguish dendrites from the melt precisely. Any modifications made to the single-phase turbulence closures must satisfy two limiting conditions on the phase boundaries. The model should reduce the eddy viscosity and thermal conductivity to their respective molecular values along the solidus line; the formula should also merge with the single-phase turbulence model within the pure melt in a smooth manner. Based on these requirements, a modified eddy viscosity formula is proposed for the present phase change problem. Firstly, the standard forms of the transport equations for the turbulent kinetic energy, k, and the rate of dissipation of turbulent kinetic energy, ε, as given by Launder and Spalding [21], are adopted.

The eddy viscosity, μ_t, is determined according to the following formula:

$$\mu_t = \frac{C_\mu \rho k^2}{\varepsilon}.$$

The original value of the coefficient C_μ proposed by Launder and Spalding is 0.09. Later, in order to accommodate the region of relatively low turbulent Reynolds number, various works suggest that C_μ be modified as

$$C_\mu = 0.09 f_\mu.$$

The function f_μ represents the generalized damping mechanism of turbulent transport in both the pure melt and the mushy zone. A number of low Reynolds number k–ε models for single-phase flows have been proposed and tested [24–27]. Here, in order to satisfy the previously stated requirements arising from phase change, it is proposed that a correlation between f_μ and liquid fraction λ be used, namely

$$f_\mu = \sqrt{\lambda} \cdot f_R$$

where

$$f_R = \exp\left[\frac{-3.4}{\left(1+\frac{R_t}{50}\right)^2}\right]$$

$$R_t = \frac{\rho k^2}{\mu \varepsilon}$$

where μ is the molecular viscosity. The function f_R represents the damping mechanism of the single-phase flow, which depends on the local turbulent Reynolds number, R_t. The formula of f_R was originally proposed by Launder and Sharma [26, 27], and has yielded more satisfactory performance for various problems [24]. A turbulent Prandtl number of 0.8 is used for all cases studied. Similar to other low Reynolds number models, there is no firm theoretical basis to 'prove' the correctness of the above form of f_μ. The test invariably comes from theory and data assessment. As will be discussed later, this modification does seem to yield solutions consistent with available experimental information.

The above set of equations is solved using a pressure-correction type of semi-implicit finite volume formulation in arbitrary curvilinear coordinates [28, 29]. The convection terms in the momentum equations are approximated by the second-order upwind scheme. The pressure as well as all the second-order derivative terms are discretized by the second-order central difference schemes. An adaptive grid method previously developed [30] is extended and applied here. The method is based on the multiple one-dimensional procedure of equidistribution. The weighting function is comprised of the contributions from the smoothness constraint, and combined velocity and temperature gradients. The original method treats the flow variable variations along each family of coordinates independently. In the present work, the Laplace equation is used as the postprocessor to improve the mesh skewness. The Laplace equation is solved by a point-SOR procedure [28]. It is well established that the point-SOR method can first eliminate the high wave number parts of error during the course of iteration. It is relatively slow in overall convergence. Hence, by utilizing the procedure for, say, five to ten iterations, the resulting grid system can exhibit improved control of grid skewness while largely retaining the same clustering characteristics, both desirable for our purpose. A nonuniform grid system with 81×81 nodes covering the whole computational domain is used.

Next we discuss the boundary conditions adopted here. Due to the fact that there is a volume shrinkage as the material solidifies, the solid portion of the ingot does not contact the copper mold even though the melt and mushy zone do. Hence, in a vacuum environment such as for EBM operation, the only energy transfer mode out of the solid material is radiation. For the liquid phase and mushy zone, a combined convection–conduction heat transfer process takes place to release heat toward the copper mold. On the top surface, the melt, on the one hand, received energy through electron beam bombardment from above and, on the other hand, released energy through radiation to the surroundings. As a simplification, vaporization has not been included in this formulation. A gray body radiation heat transfer model is adopted for both the solid boundary (on the cylindrical surface) and the liquid boundary (on the top surface). The boundary conditions of velocity and enthalpy are given below.

2.1. *For the heat transfer along the side boundaries*

(a) If $T < T_{sol}$, then the temperature and velocity boundary conditions are, respectively,

(i) Temperature

$$-k_t \left.\frac{\partial T}{\partial r}\right|_{r=R} = \sigma\varepsilon_s(T^4 - T_{mold}^4)|_{r=R}, \quad x \geqslant (L - L_{mold})$$

or

$$-k_t \left.\frac{\partial T}{\partial r}\right|_{r=R} = \sigma\varepsilon_s(T^4 - T_{amb}^4)|_{r=R}, \quad x < (L - L_{mold})$$

where σ is the Stefan–Boltzmann constant, 5.667×10^{-8} W m^{-2} K^{-4}, and ε_s is the emissivity of the solid surface; T_{mold} and T_{amb} represent, respectively, the surface temperature of the copper mold and ambient temperature. The ingot length is L and the copper mold length is L_{mold}.

(ii) Velocity

$$u(x, R) = 0, \quad v(x, R) = 0.$$

(b) if $T \geqslant T_{sol}$, then

(i) Temperature

$$-k_t \left.\frac{\partial T}{\partial r}\right|_{r=R} = h_{eff}(T - T_{mold})|_{r=R}$$

where h_{eff} is the effective contact heat transfer coefficient between mold and ingot.

(ii) Velocity

$$u(x, R) = -u_{cast}, \quad v(x, R) = 0.$$

2.2. *For the bottom surface, i.e.* $x = 0$

(a) Temperature

$$\left.\frac{\partial T}{\partial x}\right|_{x=0} = 0.$$

(b) Velocity

$$u(0, r) = 0, \quad v(0, r) = 0.$$

2.3. *For the top boundary,* $x = L$

The free surface was considered to be flat, which was a reasonable approximation according to the visualization made in the laboratory, and there were different temperature boundary conditions caused by the presence of an electron beam, namely the following.

(a) Temperature

(i) If $r_1 \leqslant r \leqslant r_2$, then the material received energy from the electron beam and lost energy through radiation to the ambient

$$-k_t \left.\frac{\partial T}{\partial x}\right|_{x=L} = q_{beam} - \sigma\varepsilon_l(T^4 - T_{amb}^4)|_{x=L}$$

where q_{beam} is the heat flux into the melt from the electron beam, and ε_l is the emissivity of liquid.

(ii) If $r < r_1$ or $r_2 < r < r_f$, where r_f is the inner radius of the annular ring for pouring, then the material loses energy through radiation

$$k_t \left.\frac{\partial T}{\partial x}\right|_{x=L} = \sigma\varepsilon_l(T^4 - T_{amb}^4)|_{x=L}.$$

(iii) If $r_f < r < R$, then the boundary received energy from material poured into the mold, and the temperature there is prescribed, i.e.

$$T(L, r_f < r < R) = T_i.$$

(b) The shear stress is balanced by the surface tension, γ, on the top boundary, i.e.

$$\mu \left.\frac{\partial v}{\partial x}\right|_{x=L} = \frac{\partial \gamma}{\partial T}\frac{\partial T}{\partial r}, \quad 0 \leqslant r \leqslant R$$

$$u(L, r) = 0.$$

Table 1 summarizes the important parameters used in the present study.

3. RESULTS AND DISCUSSION

Calculations have been conducted for cases that contain full contributions of both buoyancy and surface tension, and that contain only the surface tension effect. With such a systematic scrutiny, both the collective and individual effects of the two convection mechanisms can be investigated, and their interaction with solidification studied. The results presented in the following correspond to two casting speeds: -2×10^{-4} m s^{-1} (455 kg h^{-1}) and -4×10^{-4} m s^{-1} (910 kg h^{-1}), and under the influence of two gravity levels, one the standard value (g_0) measured on earth (termed the earth-bound condition), and the other $10^{-5}\, g_0$ (termed the microgravity condition). Figure 2 shows the adaptive grid distribution generated for each case. To generate the grid, explicit phase boundary tracking method may not be well suited here for the reason that, in the context of isothermal phase change, the phase boundaries only correspond to the temperature contours, and are not related directly to the convection field. The domain decomposition practice adopted for pure material single crystal growth [31, 32] that divides the overall domain into separate zones according to the phase boundaries is not used here. Instead, the whole domain is considered as a single zone, and the grid is generated based on the aforementioned adaptive technique. As demonstrated in Fig. 2, for cases under the normal gravity level, adequate spatial resolution is needed for both enthalpy and stream function in the melt and mushy zone since the convection is strong. Consequently, the grid lines do not directly correlate with the phase boundaries. Under microgravity, on the other hand, the convection field is much reduced, and hence the grid lines can more directly correspond to the characteristics of the thermal field, as is discussed later. As one can clearly observe from Fig. 2, the higher the casting speed, the more downward the solidus line.

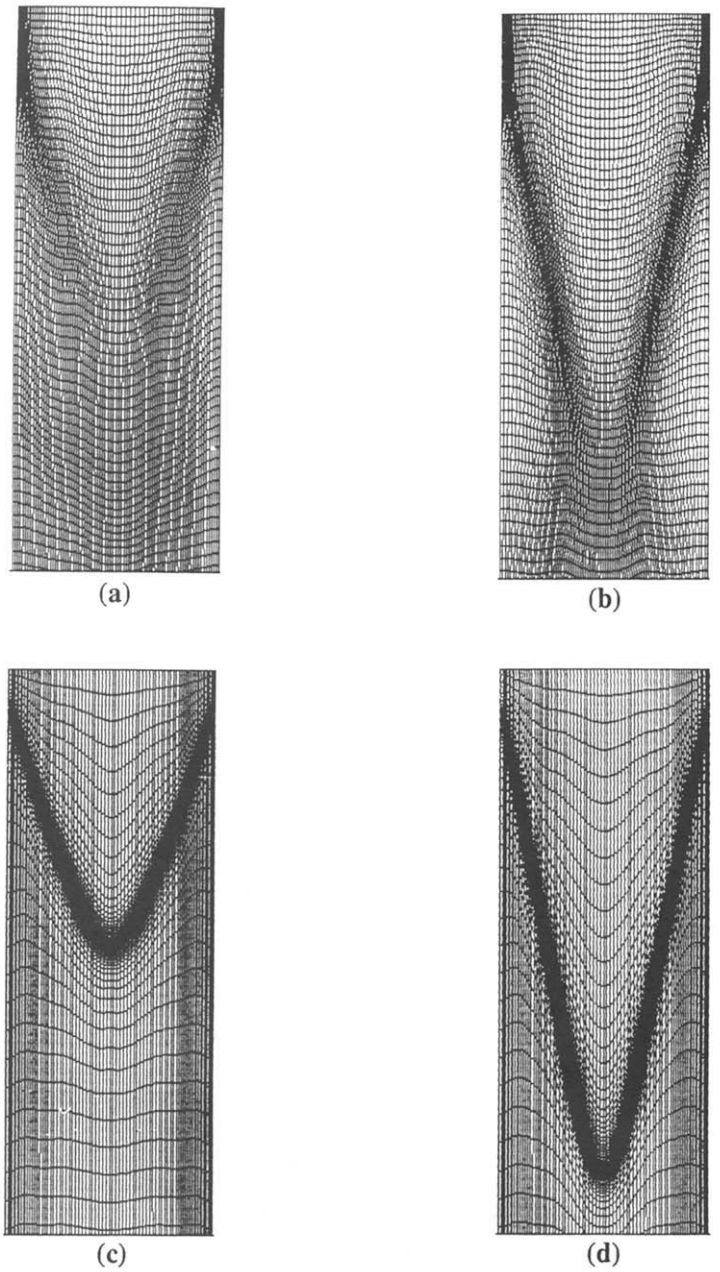

FIG. 2. Adaptive grid distributions corresponding to modeling condition (only upper portion of domain is shown). (a) Normal gravity, $u_{cast} = -2 \times 10^{-4}$ m s^{-1}. (b) Normal gravity, $u_{cast} = -4 \times 10^{-4}$ m s^{-1}. (c) Microgravity, $u_{cast} = -2 \times 10^{-4}$ m s^{-1}. (d) Microgravity, $u_{cast} = -4 \times 10^{-4}$ m s^{-1}.

The meshes around the solidification interface tend to be less orthogonal, most noticeably for the case of $u_{cast} = -4 \times 10^{-4}$ m s^{-1} and under microgravity. This mesh distribution is formed because convection under the given condition is relatively weak, and hence the grid clustering is needed primarily for tracking the phase boundaries where the latent heat release is significant. As demonstrated in a previous study [33], under such a circumstance, it is good practice to emphasize length scale resolution above mesh orthogonality.

Figures 3–5 present various aspects of solutions obtained under the normal gravity level, including isotherms, liquid fraction distribution across the mushy zone, convection field, and turbulence structures. Two different casting speeds have been used for computations to investigate their impact on the resulting solidification characteristics. Compared to the solutions obtained previously with a simple zero-equation turbulence model [19], the present results show both similarity and differences. Selected plots depicting the liquid fraction contours under different conditions as predicted by the zero-equation turbulence model are collected from ref. [19] and shown

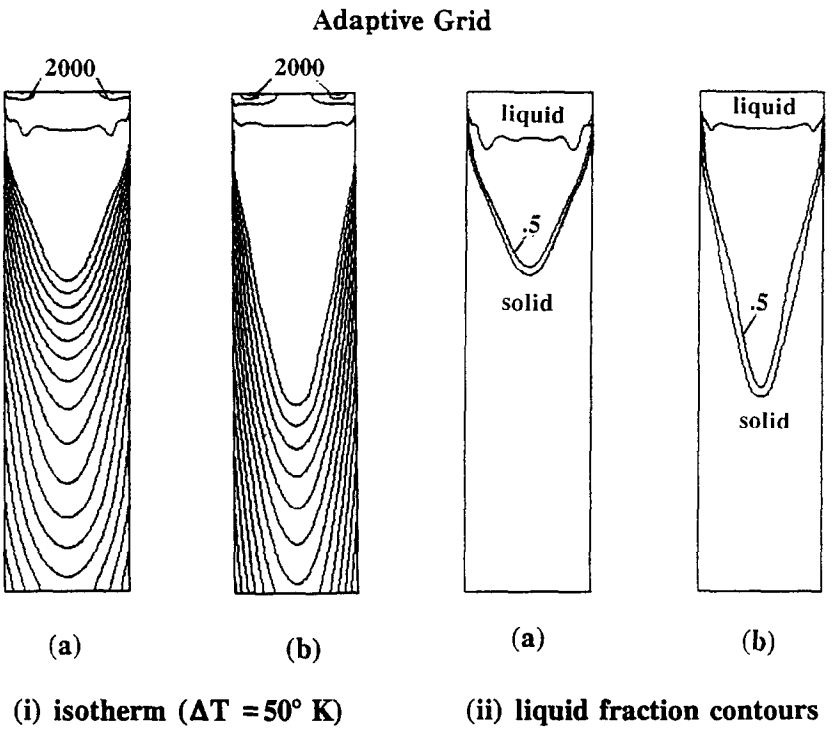

FIG. 3. Effect of casting speed on temperature and liquid fraction contours as predicted by modified k–ε turbulence model and under normal gravity. (a) $u_{cast} = -2 \times 10^{-4}$ m s^{-1}. (b) $u_{cast} = -4 \times 10^{-4}$ m s^{-1}.

in Fig. 6 for comparison. Qualitatively, both models predict a thick mushy zone as a result of the convection effect, and the zone thickness varies with the change of casting speed. Within the half domain of the cross-section, both models predict that contrarotating eddies appear, albeit with different strengths and number of eddies, due to the combined effects of surface tension and buoyancy. The liquidus line in both solutions is approximately flat, and its depth appears to be insensitive to the variation of the casting speed. Quantitatively, on the other hand, distinctive differences are readily observable between the solutions yielded by the present modified k–ε and previous zero-equation turbulence models. Not only do the present solutions exhibit solidus lines of higher curvature, but also the temperature gradients vary more non-uniformly from solidus to liquidus lines. Previously, the solidus line was of a more rounded shape, and the temperature profile changed very smoothly across the mushy zone.

The modified k–ε model has produced solutions more consistent with our expectation in one important aspect, namely, the thermal characteristics between 50% liquidus and solidus lines. Under a given set of thermal energy conditions, the mushy zone yielded by the pure conduction transport, shown in Fig. 6(i), is generally thin in order to maintain required heat flow rates by the microscopic molecular mechanism, i.e. conduction, alone. With the inclusion of convection, the heat transfer rates in both the bulk melt and upper mushy zone are now enhanced by macroscopic flow motion; the degree of heat transfer enhancement depends, of course, on the local convection strength. In the bulk melt as well as the upper mushy zone where convection is vigorous, turbulence plays a dominant role in overall heat transfer, and accordingly, in these regions the temperature distribution is smeared and the overall thermal gradients are much reduced. Toward the solidus lines, however, the increasing presence of the solidified dendrites within the mushy zone dampens convection, and the thermal conduction again becomes the controlling mechanism. This change of dominant transport mechanism from liquidus to solidus line explains why in regions close to the solidus line the temperature gradients are high, resulting in small mushy zone thicknesses encompassing large variations of the liquid fraction; while, on the other hand, close to the liquidus line the temperature gradients are low, resulting in much increased mushy zone thicknesses there. These features were not realized previously by the zero-equation turbulence model since the interactions between convection and dendrite damping in the mushy zone were not directly accounted for.

Figure 4 shows the distribution of stream function and eddy viscosity under the two casting speeds. Although the patterns of the distributions appear qualitatively the same for both speeds, it is clear that the higher the casting speed, the deeper the convection penetration into the mushy zone. With regard to the

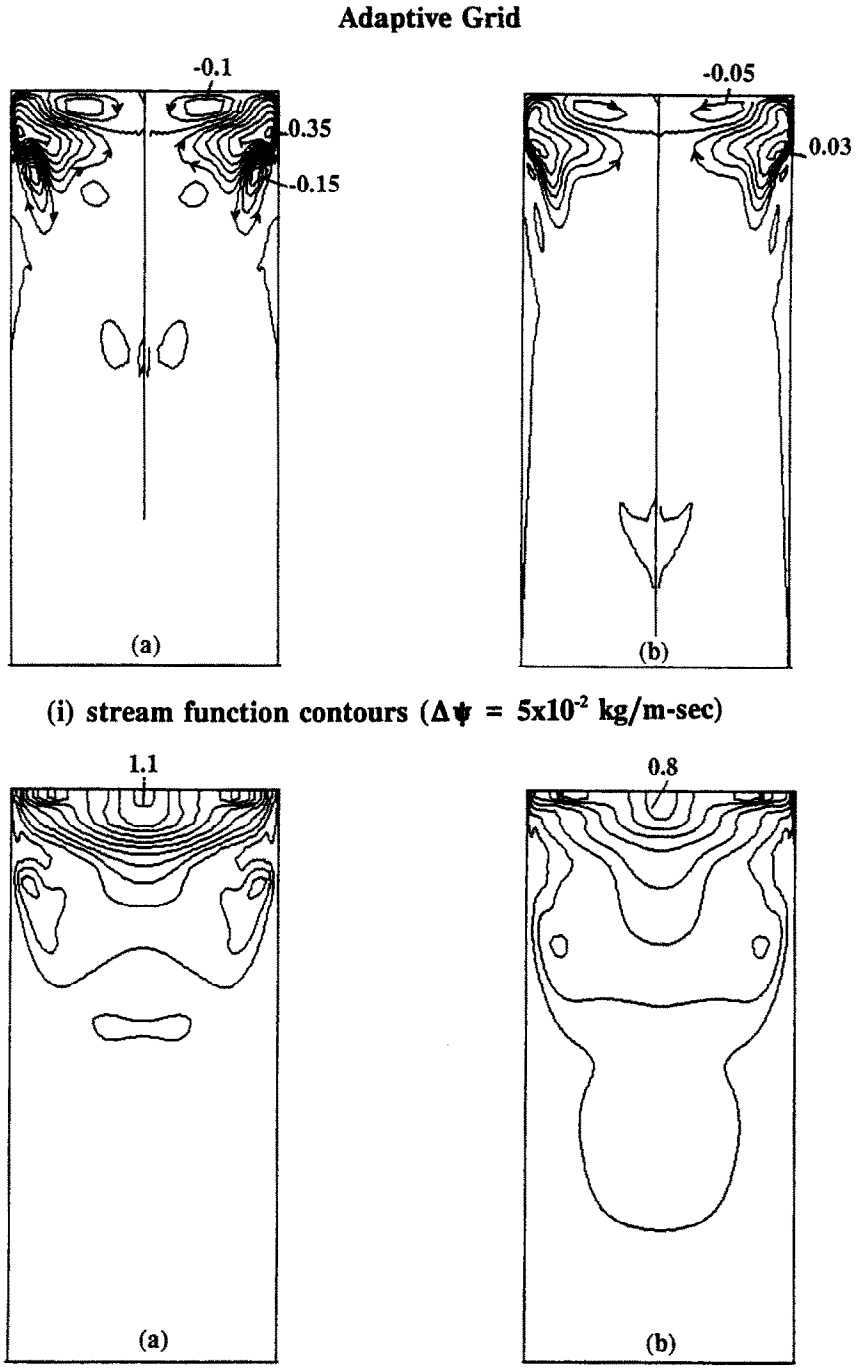

FIG. 4. Effect of casting speed on stream function and eddy viscosity contours as predicted by modified k–ε turbulence model and under normal gravity (only upper portion of domain is shown). (a) $u_{cast} = -2 \times 10^{-4}$ m s^{-1}. (b) $u_{cast} = -4 \times 10^{-4}$ m s^{-1}.

eddy viscosity, its distribution in the mushy zone reflects the greater convection effect there. Energy input from the electron beam and superheated incoming melt, as indicated in Fig. 1(b), on the distribution of μ_t can also be clearly observed. In fact, the rings of electron beam bombardment and incoming melt are the regions where both the production and the dissipation of the turbulent kinetic energy reach the highest levels, as demonstrated in Fig. 5. This feature may be intuitive, but it could not, of course, be predicted using the previous zero-equation turbulence model.

The solutions obtained with the identical modeling condition and physical models, but under a micro-

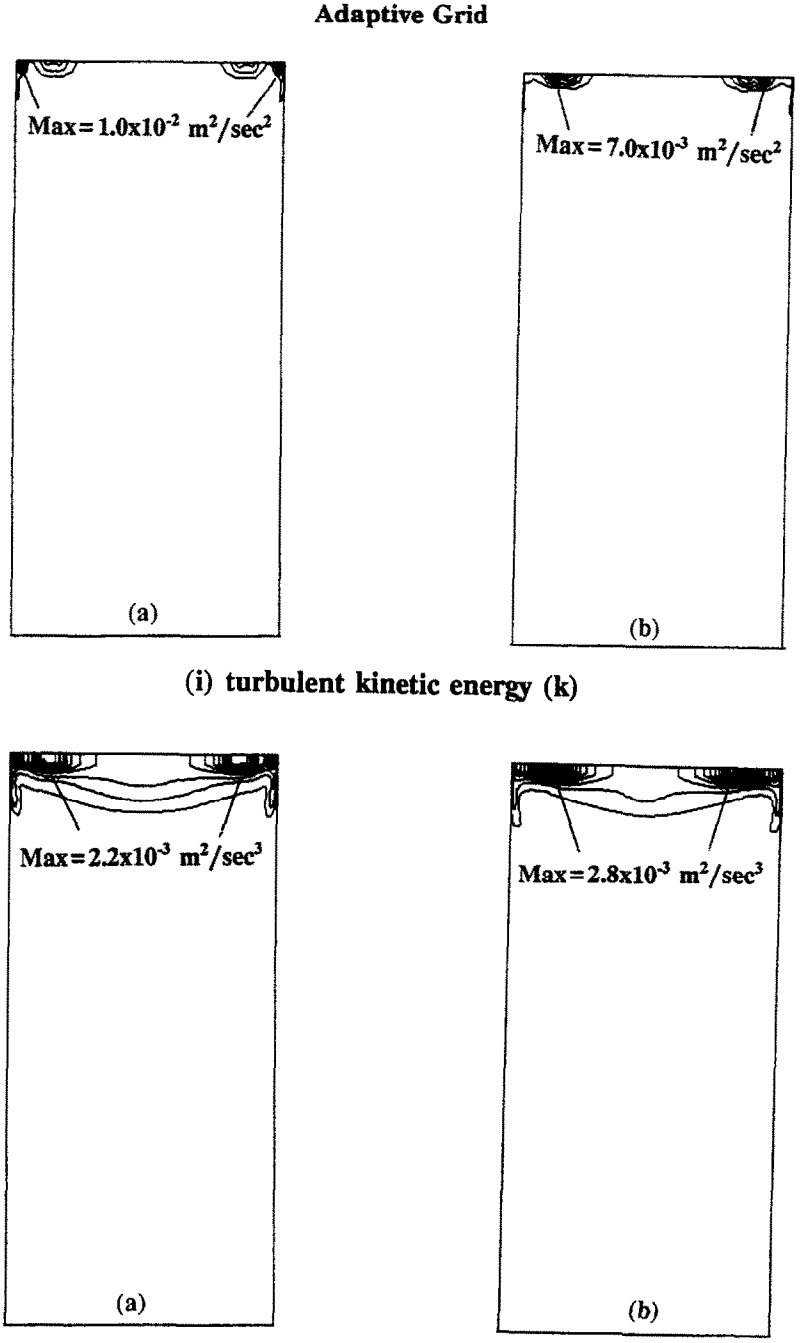

FIG. 5. Effect of casting speed on turbulent kinetic energy and dissipation rate of turbulent kinetic energy contours as predicted by modified k–ε turbulence model and under normal gravity (only upper portion of domain is shown). (a) $u_{cast} = -2 \times 10^{-4}$ m s^{-1}. (b) $u_{cast} = -4 \times 10^{-4}$ m s^{-1}.

gravity condition with 10^{-5} times the gravity level on earth, are presented next. Although the gross qualitative features between the solutions shown in Fig. 7 and those in ref. [19], summarized in Fig. 6(iii), are again similar, the differences for cases under microgravity are larger than those under earth-bound conditions. Figure 7 shows that, under microgravity, the mushy zones are generally of much reduced thickness than those under the normal gravity level. Under microgravity, the convection strength, all produced virtually by the surface tension alone, is much weaker. Consequently, the liquidus line tends to have a stronger curvature, and the solidus line corresponding to the same casting speed is deeper than under normal gravity.

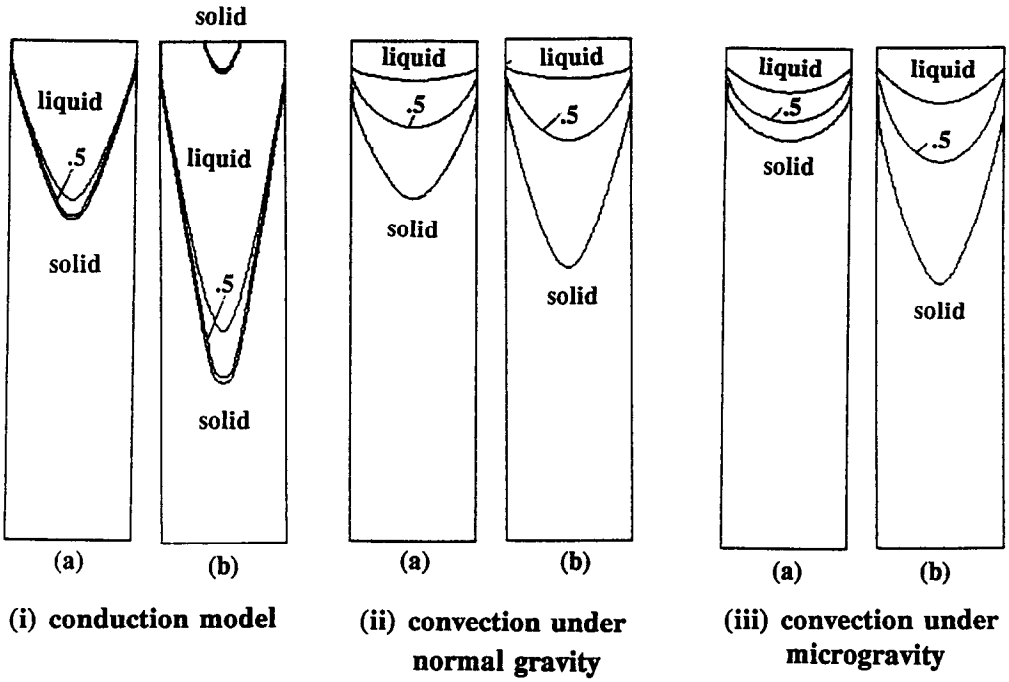

FIG. 6. Liquid fraction contours ($\Delta\lambda = 0.5$) as predicted by conduction model (i) and zero-equation turbulence model under normal (ii) and microgravity (iii) conditions, and two casting speeds: (a) $u_{cast} = -2 \times 10^{-4}$ m s^{-1}; (b) $u_{cast} = -4 \times 10^{-4}$ m s^{-1}. (From AIAA-91-0506, ref. [19].)

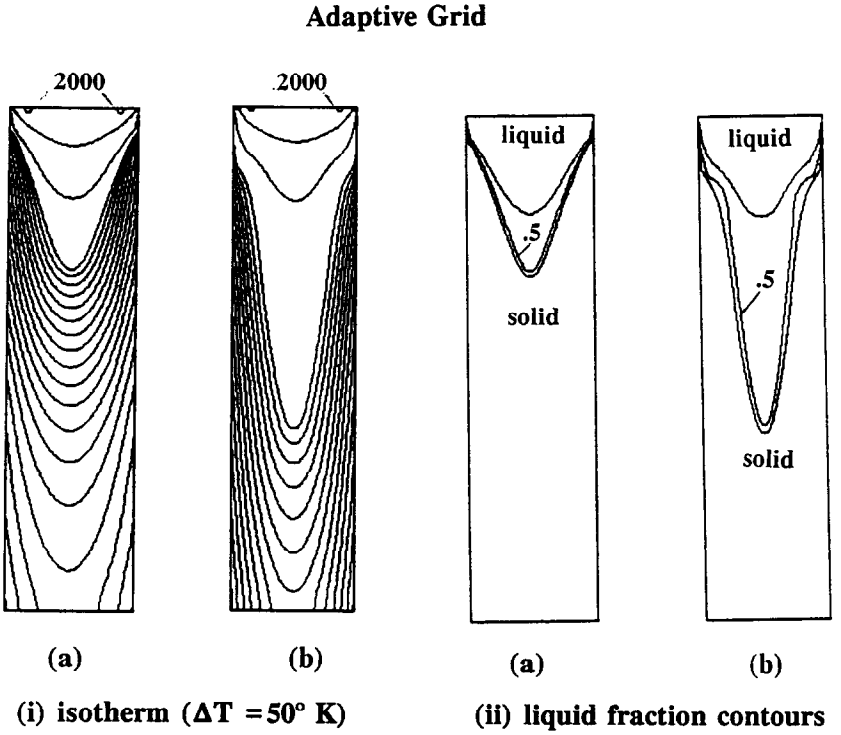

FIG. 7. Effect of casting speed on temperature and liquid fraction contours as predicted by modified k–ε turbulence model and under microgravity. (a) $u_{cast} = -2 \times 10^{-4}$ m s^{-1}. (b) $u_{cast} = -4 \times 10^{-4}$ m s^{-1}.

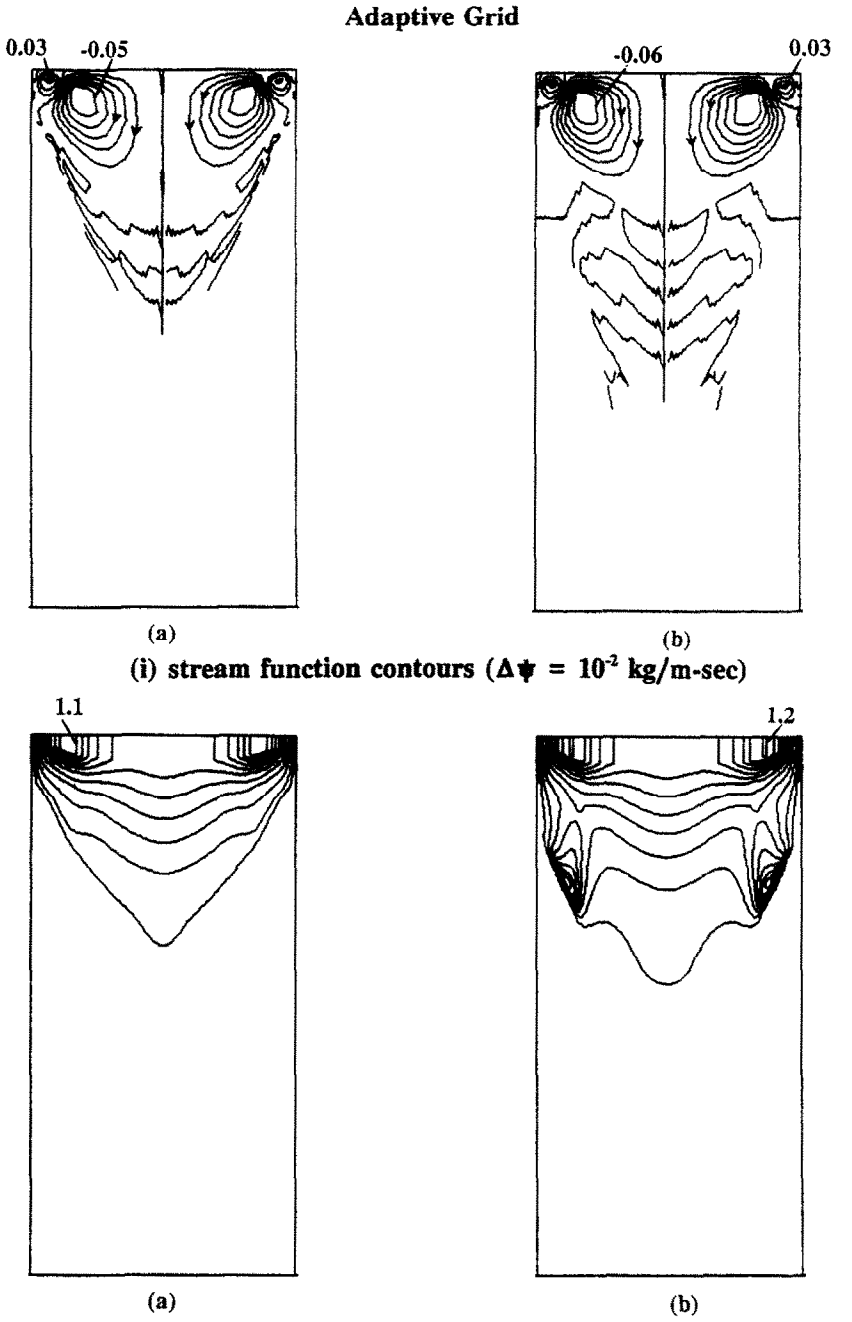

FIG. 8. Effect of casting speed on stream function and eddy viscosity contours as predicted by modified k–ε turbulence model and under microgravity (only upper portion of domain is shown). (a) $u_{cast} = -2 \times 10^{-4}$ m s^{-1}. (b) $u_{cast} = -4 \times 10^{-4}$ m s^{-1}.

Stream function and eddy viscosity distributions are shown in Fig. 8. Within the mushy zone, some very weak convection cells can be observed. Similar to the earth-bound conditions, contrarotating eddies can be observed within the melt for the present microgravity condition, albeit of much reduced strength. This convection pattern is different from that observed with the zero-equation turbulence model [19], where only a single primary convection cell, instead of a pair, can be found in the melt. The pattern of eddy viscosity distribution is again controlled largely by the combined effects of convection and incoming heat sources from the feeding melt and electron beam. It is interesting to note that the energy input from the electron beam and superheated feeding melt plays such a dominant effect that despite very different characteristics of mushy zone and thermal and convection fields exhibited between solutions under

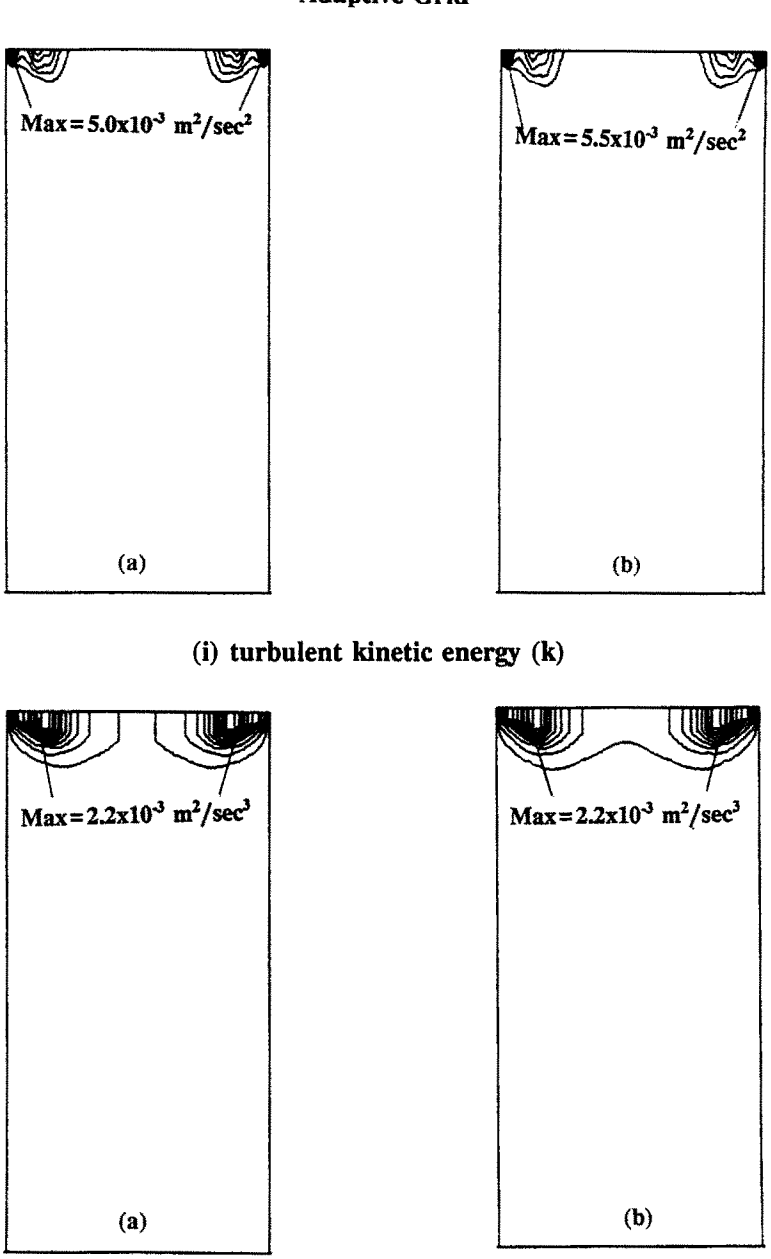

FIG. 9. Effect of casting speed on turbulent kinetic energy and dissipation rate of turbulent kinetic energy contours as predicted by modified k–ε turbulence model and under microgravity (only upper portion of domain is shown). (a) $u_{cast} = -2 \times 10^{-4}$ m s^{-1}. (b) $u_{cast} = -4 \times 10^{-4}$ m s^{-1}.

normal and reduced gravity levels, the distributions of k and ε (Figs. 5 and 9) of the two conditions are concentrated similarly in regions of the electron beam impingement and melt pouring. These distributions are also concentrated similarly on the top surface at the mold wall due to surface tension driven flows, although the concentration is higher for the earth-bound condition due to increased buoyancy strength.

4. COMPARISON WITH EXPERIMENTAL OBSERVATION

Besides studying the general characteristics of the solidification process, an important goal of this program is to develop a predictive capability for the resulting ingot structure given various process parameters. Attempts to achieve this capability using a

classical phase change conduction formulation have been instructive, but have not been fully satisfactory. The numerical techniques described herein are an ongoing part of a development effort to improve the predictive capability. A necessary part of this development is to compare the numerical results to available experimental evidence.

A Ti–6Al–4V ingot was cast in an EBM process with the process parameters that were simplified as shown in Fig. 1(b). The casting rate, u_{cast}, was approximately -1.8×10^{-4} m s^{-1}. A small amount of copper was added to the ingot mold pool near the end of the casting process to mark the pool profile for subsequent ingot macroetch evaluation. The ingot top was sliced axially, and the slices were macroetched by standard nitric–hydrofluoric and ammonium bifluoride etchants. The result, shown in Fig. 10, includes an outline trace of the pool profile for added clarity.

Given experimental uncertainties, the maximum depth of the pool profile is assessed as 53 cm. Because it reduces the melting temperature, the copper probably caused some of the solid, particularly in the mushy zone, to remelt. Since there was insufficient heat available to remelt much of the solid, the profile indicated by macroetching is probably close to the solidus line. The orientation of the columnar dendritic structure that does not contain copper suggests that the macroetch profile at least approximates the solidus line.

The modified k–ε turbulence model prediction for the solidus line profile has features which correlate to features observed on the macroetch profile. The 'bulge' outward in the upper portion of the pool appears qualitatively in both profiles. This feature does not appear in the conduction only and zero-equation turbulence model predictions. The high curvature at the bottom of the macroetch pool profile also corresponds more closely to the modified k–ε turbulence model than the zero-equation model. As predicted with both turbulence models, the pool depth is roughly proportional to the casting rate. Therefore, the pool depth predicted by the modified k–ε turbulence model of 61 cm in Fig. 3(ii) is adjusted to 55 cm to correspond with the -1.8×10^{-4} m s^{-1} casting rate. The 55 cm prediction closely approximates the macroetch profile depth of 53 cm.

The modified turbulence convection model results show that progress is being made toward a predictive capability. Comparison between the numerical and experimental results indicates that more work still remains. All of the numerical predictions have a much thinner solid layer near the top pool surface and a lower curvature at the pool bottom than observed in the macroetch profile. It is not known if this is because the h_{eff} estimate is too low or the models fail to include some critical mechanisms. More efforts are required, both experimentally and theoretically, to determine the detailed thermal characteristics associated with the phase change process and to investigate their relationships with the columnar dendritic structure observed below the macroetch profile as shown in Fig. 10. Issues such as the estimates of mushy zone characteristics, turbulence behavior, material properties, and process parameters need to be addressed with more quantitative information. Furthermore, the axisymmetric models cannot predict the asymmetric features observed in the macroetch profile, which probably relate to the pour entry location.

5. SUMMARY AND CONCLUSION

A modified k–ε turbulence model is developed and applied to compute the interaction between convection and phase change characteristics during continuous ingot casting. The model is developed in conjunction with the modification made to the Navier–Stokes equations by Darcy's terms and the enthalpy formulation. Computations aided by the adaptive grid technique have been conducted for cases corresponding to two different casting speeds, under both earth-bound and microgravity conditions. Assessments are made between the present solutions and the previous solutions obtained using a simple zero-equation turbulence model [19]. Based on the results obtained and discussed, it is found that some qualitative features predicted by both turbulence models are similar, including a generally thick mushy zone and the strong effect of the casting speed on the mushy zone thickness. However, the shape as well as the curvature of both liquidus and solidus lines predicted by the two models are different. The modified k–ε model yields a solidus line generally of sharper curvature. This feature appears to be more consistent with the experimental observation. The modified model also produces much higher temperature gradients close to the solid boundary, which is consistent with reduced convection in the mushy zone.

Across the mushy zone and within the melt, although the thermal characteristics affect the turbulent transport, the modified k–ε model shows that, as expected, no direct correspondence exists between μ_t and temperature contours, which is the basis of the zero-equation model used in ref. [19]. The energy input from the superheated feeding melt and the electron beam is very influential not only on maintaining the melt size, but also on the generation and dissipation of the turbulent kinetic energy. Consequently, convection and the electron beam collectively appear to exhibit the most influence on the distribution of eddy viscosity for all cases considered.

Under microgravity, the modified k–ε model results in a melt pool of much stronger curvature and hence a larger melt volume, due to the reduced convection strength. The dominant effect of the feeding melt and electron beam on the distribution of k and ε, however, remains the same for both gravity levels.

Compared to previous ingot casting models, it appears that the present modified k–ε model is more comprehensive, capable of incorporating the effects of both convection and temperature fields, and exhibits a

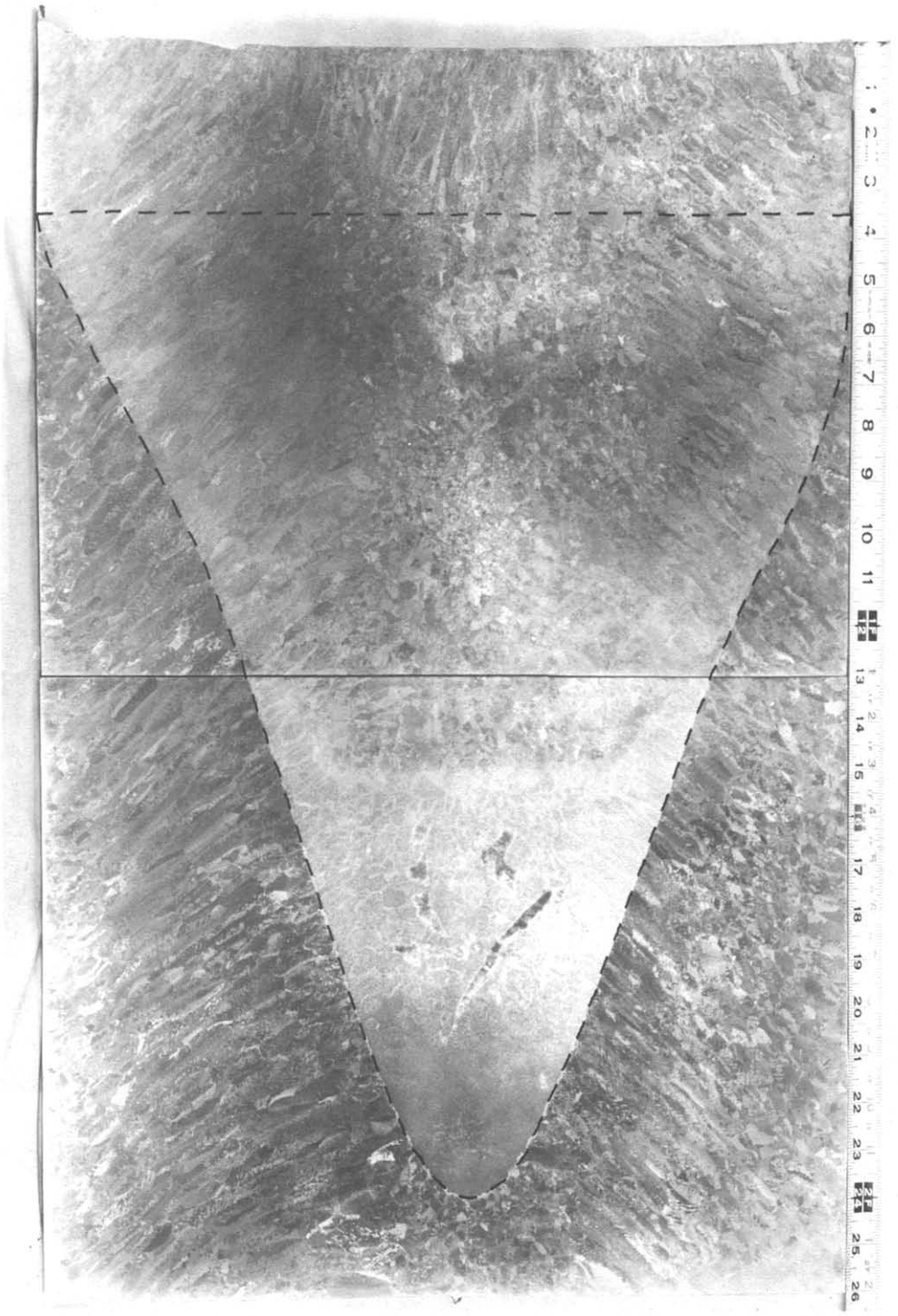

FIG. 10. Macroetched axial pool profile from the ingot mold (pour entry on left).

high degree of responsiveness with respect to the high energy input of the electron beam and the variation of the casting speed. Based on the present model, more insights on the interactions among convection, thermal transport, and phase change have been gained, and a more definite assessment of both the casting speed and the gravity level has been made.

Acknowledgements—The authors are pleased to acknowledge that some of the computations were made using the CRAY-XMP/48 of the National Center for Supercomputer Applications (NCSA) at the University of Illinois through a research grant, and that the experimental determination of an ingot mold pool profile was conducted as part of contract F33615-88-C-5418 from the U.S. Air Force Manufacturing Technology Directorate, Wright Laboratory.

REFERENCES

1. C. E. Shamblen and G. B. Hunter, Titanium base alloys clean melt process development. In *Proc. 1989 Vacuum Metallurgy Conf.* (Edited by L. W. Lherbier and J. T. Cordy), pp. 3–11. Iron and Steel Society, Warrendale, PA (1989).
2. G. E. Maurer, Primary and secondary melt processing–Superalloy. In *Superalloys, Supercomposites and Superceramics* (Edited by J. K. Tien and T. Caulfield), pp. 49 97. Academic Press, New York (1989).
3. D. G. Backman, Metal–matrix composites and IPM: a modeling perspective, *J. Metals* July, 17–20 (1990).
4. D. W. Tripp and A. Mitchell, Segregation and hot-topping of titanium alloy ingots. In *Proc. 1989 Vacuum Metallurgy Conf.* (Edited by L. W. Lherbier and J. T. Cordy), pp. 83–88. Iron and Steel Society, Warrendale, PA (1989).
5. F. Rosenberger, *Fundamentals of Crystal Growth I*, Chap. 5. Springer, Berlin (1979).
6. S. Ostrach, Fluid mechanics in crystal growth, *ASME J. Fluids Engng* **105,** 5–20 (1983).
7. R. A. Brown, Theory of transport processes in single crystal growth from the melt, *A.I.Ch.E. Jl* **34,** 881–911 (1988).
8. S. H. Davis, Hydrodynamic interactions in directional solidification, *J. Fluid Mech.* **212,** 241–262 (1990).
9. M. J. Crochet, F. Dupret, Y. Ryckmans, F. T. Ceyling and E. M. Monberg, Numerical simulation of crystal growth in a vertical bridgman furnace, *J. Crystal Growth* **97,** 173 185 (1987).
10. M. E. Thompson and J. Szekely, The transient behavior of weldpools with a deformed free surface, *Int. J. Heat Mass Transfer* **32,** 1007–1019 (1989).
11. M. S. Christenson, W. D. Bennon and F. P. Incropera, Solidification of an aqueous ammonium chloride solution in a rectangular cavity—II. Comparison of predicted and measured results, *Int. J. Heat Mass Transfer* **32,** 69–79 (1989).
12. C. Beckermann and R. Viskanta, Double-diffusive convection due to melting, *Int. J. Heat Mass Transfer* **31,** 2077–2089 (1988).
13. V. R. Voller and C. Prakash, A fixed grid numerical modeling methodology for convection–diffusion mushy region phase-change problems, *Int. J. Heat Mass Transfer* **30,** 1709–1719 (1987).
14. M. E. Thompson and J. Szekely, Mathematical and physical modeling of double-diffusive convection of aqueous solution crystallizing at a vertical wall, *J. Fluid Mech.* **187,** 409–433 (1988).
15. W. Shyy and M.-H. Chen, Effect of Prandtl number on buoyancy-induced transport processes with and without solidification, *Int. J. Heat Mass Transfer* **33,** 2565–2578 (1990).
16. J. A. Dantzig, Modeling liquid–solid phase change with melt convection, *Int. J. Numer. Meth. Engng* **28,** 1769–1785 (1989).
17. J. C. Heinrich, S. Felicelli, P. Nadapukar and D. R. Poirier, Thermosolutal convection during dendritic solidification of alloys, part II: nonlinear convection, *Metall. Trans* **20B,** 883–891 (1989).
18. A. Mitchell and S. Joshi, The thermal characteristics of the electroslag process, *Metall. Trans.* **4,** 631–642 (1973).
19. W. Shyy, Y. Pang, D. Y. Wei and M.-H. Chen, Effects of surface tension and buoyancy on continuous ingot solidification, AIAA 28th Aerospace Science Meeting, Paper No. 91-0506 (1991).
20. A. Murthy, J. Szekely and N. El-Kaddah, Experimental measurement and numerical computation of velocity and turbulence parameters in a heated liquid metal system, *Metall. Trans.* **18B,** 765–775 (1988).
21. B. E. Launder and D. B. Spalding, The numerical computation of turbulent flows, *Comput. Meth. Appl. Mech. Engng* **3,** 269–289 (1974).
22. W. P. Jones and B. E. Launder, The prediction of laminarization with a two-equation model of turbulence, *Int. J. Heat Mass Transfer* **15,** 301–314 (1972).
23. P. N. Quested and M. Mclean, Solidification morphologies in directionally solidified superalloys, *Mater. Sci. Engng* **65,** 171–180 (1984).
24. V. C. Patel, W. Rodi and G. Scheuerer, Turbulence models for near-wall and low Reynolds number flows: a review, *AIAA J.* **23,** 1308–1319 (1985).
25. C. K. G. Lam and K. A. Bremhorst, A modified form of the k–ε model for predicting wall turbulence, *ASME J. Fluids Engng* **103,** 456–460 (1981).
26. B. E. Launder and B. I. Sharma, Application of the energy dissipation model of turbulence to the calculation of flow near a spinning disc, *Lett. Heat Mass Transfer* **1,** 131–138 (1974).
27. B. E. Launder, On the computation of convective heat transfer in complex turbulent flows, *ASME J. Heat Transfer* **110,** 1112–1128 (1988).
28. W. Shyy, S. S. Tong and S. M. Correa, Numerical recirculating flow calculation using a body-fitted coordinate system, *Numer. Heat Transfer* **8,** 99–113 (1985).
29. W. Shyy, S. M. Correa and M. E. Braaten, Computation of flow in a gas turbine combustor, *Combust. Sci. Technol.* **58,** 97–118 (1988).
30. W. Shyy, Computation of complex fluid flows using an adaptive grid method, *Int. J. Numer. Meth. Fluids* **8,** 475–489 (1988).
31. Y. T. Chan, H. J. Gibeling and H. L. Grubin, Numerical simulations of Czochralski silicon growth, *J. Appl. Phys.* **64,** 1425–1439 (1988).
32. C. W. Lan and S. Kou, Thermocapillary flow and melt/solid interfaces in floating-zone crystal growth under microgravity, *J. Crystal Growth* **102,** 1043–1058 (1990).
33. W. Shyy and M. E. Braaten, Applications of a generalized pressure correction algorithm for flows in complicated geometries. In *Advances and Applications in Computational Fluid Dynamics* (Edited by O. Baylsal), FED-Vol. 66, pp. 109–119. ASME, New York (1988).

MODELISATION DU TRANSPORT TURBULENT ET DE LA SOLIDIFICATION PENDANT LA COULEE CONTINUE DES LINGOTS

Résumé—La coulée continue est un procédé important pour plusieurs matériaux dans lequel la turbulence joue un rôle critique avec les mécanismes de transport tels que le flottement, la tension interfaciale, le changement de phase, ce qui influe sur la qualité des produits finis. On propose un modèle de turbulence k–ε avec fermeture à deux équations et on l'applique à la prédiction du changement de phase et des caractéristiques de convection–diffusion pendant la coulée d'un lingot d'alliage de titane. En rapport avec une technique adaptative de maillage, les solutions des équations des bilans sont obtenues à partir de la formulation enthalpique. On peut prédire que la zone de bouillie a généralement une épaisseur importante du fait de la convection, que la courbe de solidus a une courbure élevée et que le gradient de température près de la courbe de solidus est plus élevée qu'ailleurs. La structure de la turbulence reflète fortement l'influence combinée de la convection et de l'apport d'énergie par le faisceau électronique. Les résultats numériques sont comparés à un profil du bain expérimental par une coulée de lingot.

MODELLIERUNG DER TURBULENTEN TRANSPORT- UND ERSTARRUNGSVORGÄNGE BEIM KONTINUIERLICHEN BLOCKGIESSEN

Zusammenfassung—Das kontinuierliche Blockgießen ist eine wichtige Verarbeitungstechnik für viele Materialien. Unter den Bedingungen der praktischen Anwendung spielt die Turbulenz in Verbindung mit den Transportmechanismen (beispielsweise Auftrieb, Oberflächenspannung und Phasenwechsel) eine kritische Rolle, welche für die Qualität des Endprodukts bestimmend ist. Auf der Grundlage des Standard k–ε Zweigleichungsverfahrens wird ein modifiziertes Turbulenzmodell vorgestellt. Mit seiner Hilfe wird der Phasenwechsel und das Konvektions-Diffusionsverhalten beim Blockgießen einer Titanlegierung mittels Elektronenstrahlschmelzung berechnet. In Verbindung mit einer adaptiven Gitterberechnungsmethode werden Lösungen für die gekoppelten Bilanzgleichungen für Masse, Impuls, Energie und Turbulenz ermittelt. Dazu wird eine Enthalpieformulierung verwendet. Der Einfluß der Gießgeschwindigkeit und der Schwerkraft auf die Erstarrungs- und die Konvektionsvorgänge werden ermittelt und mit denjenigen verglichen, die sich mit einem sehr einfachen Turbulenzmodell ergeben. Das vorgeschlagene Turbulenzmodell sagt voraus, daß die Verfestigungszone aufgrund des Konvektionseffekts eine nennenswerte Dicke aufweist, daß die Soliduslinie eine starke Krümmung zeigt, und daß der Temperaturgradient nahe der Soliduslinie größer ist als an anderen Stellen. Unter allen Bedingungen spiegelt die Turbulenzstruktur deutlich die folgenden Einflüsse weder: Konvektion, Energiezufuhr durch den Elektronenstrahl und Zufuhr überhitzten Materials von der oberen Deckfläche. Die numerischen Ergebnisse werden mit experimentell an einer Blockgießanlage ermittelten Profilen verglichen.

МОДЕЛИРОВАНИЕ ТУРБУЛЕНТНОГО ПЕРЕНОСА И ЗАТВЕРДЕВАНИЯ ПРИ НЕПРЕРЫВНОЙ ОТЛИВКЕ СЛИТКОВ

Аннотация—Непрерывная отливка слитков является важным технологическим процессом при обработке многих материалов. В большинстве практических случаев турбулентность наряду с такими факторами переноса как подъемная сила, поверхностное натяжение и фазовый переход определяет качество конечных продуктов. Предложена модифицированная модель турбулентности на основе замкнутой стандартной k–ε модели, которая применяется для описания фазового перехода, а также определения характеристик конвекции и диффузии при отливке слитков титанового сплава в процессе эклектроннолучевого плавления. С использованием адаптивного сеточного метода получены решения взаимосвязанных уравнений неразрывности, имульса, энергии и турбулентного переноса в терминах энтальпии. Установлено влияние скорости отливки и силы тяжести на характеристики затвердевания и конвекции и проведено сравнение с результатами, полученными ранее с помощью простой модели турбулентности. Из предложенной модели турбулентности следует, что рыхлая зона обылая зона обычно имеет существенную толщину из-за конвекции, линия солидуса характеризуется большой, а температурный градиент наиболее высок вблизи линии солидуса. Во всех условиях структура турбулентности отражает совместное влияние конвекции и подвода мощности за счет электронного луча, а также подачи перегретого материала из верхних слоев. Численные результаты сравниваются с экспериментально определенным профилем объема расплава при отливке слитков.